Characterization of Multi-GNSS Receiver Biases and their Temperature-Induced Variations in Low Earth Orbit

Zachary Arnett, Brian C. Peters, Ryan McKnight, and Sabrina Ugazio, *Ohio University*

BIOGRAPHY

Zachary Arnett is pursuing his Ph.D. in Electrical Engineering and Computer Science at Ohio University as part of the Avionics Engineering Center. His research interests include GNSS inter-constellation time offset determination and radio-frequency pulsar navigation and timing. He received his M.S. in Electrical Engineering from Ohio University in 2023.

Brian C. Peters is pursuing his Ph.D. in Electrical Engineering and Computer Science at Ohio University as part of the Avionics Engineering Center. He completed his M.S. in Electrical Engineering at Ohio University in 2021 where he was involved in the development and operation of the Bobcat-1 CubeSat and conducted research on estimation of GNSS inter-constellation time offsets.

Ryan McKnight is a Ph.D. candidate at the Avionics Engineering Center, School of Electrical Engineering and Computer Science, Ohio University, where he has worked on PNT research since 2017. His research interests include small satellites, GNSS interoperability, GNSS interference monitoring, weak-signal GNSS, pulsar-based navigation/timing, and deep space navigation. He was previously involved with the development and operations of the Bobcat-1 CubeSat. He received his M.S. in Electrical Engineering from Ohio University in 2023.

Sabrina Ugazio is an Assistant Professor in EECS at Ohio University. She obtained her Ph.D. in Electronics and Telecommunications at Politecnico di Torino (Italy) in 2013. Her research interests include receiver design, timing, remote sensing, GNSS interoperability and space applications.

ABSTRACT

In support of full interoperability between Global Navigation Satellite Systems (GNSSs) constellations, Bobcat-1, a 3-unit CubeSat, was deployed with the primary objective of evaluating the feasibility of estimating system-to-system time offsets (XYTOs) from low Earth orbit (LEO). Bobcat-1, developed by Ohio University, was deployed in November 2020 from the International Space Station (ISS) and deorbited in April 2021 after a successful 17-month mission. The maximum orbit altitude, after deployment, was about $440\,\mathrm{km}$ and was above $380\,\mathrm{km}$ for more than a year. At these altitudes, the ionospheric effect on GNSS measurements is lower than those experienced by terrestrial users but still present; the multi-GNSS receiver onboard Bobcat-1 provides multi-frequency measurements, enabling dual-frequency ionospheric corrections. However, ionospheric corrections are affected by receiver-specific inter-frequency bias (IFB) as well as by satellite differential code biases (DCBs). These biases need to be calibrated in order to form accurate XYTOs estimates. In addition, given the significant temperature variations experienced by Bobcat-1 in orbit, the effect of temperature on the receiver-specific IFB shall be taken into account.

In this paper, the receiver-specific IFB calibration applied to Bobcat-1 is described, and the in-lab IFB temperature calibration is validated over multiple in-orbit data collections, spanning a six-month time interval. Results shown in this analysis focus on Galileo E1C-E5b and GPS L2P(Y) (semi-codeless)-L5 IFB, with plans to expand to other GNSSs and frequency/signal combinations in future work. In order to separate IFB from the ionospheric effect, a zero-total electron content (TEC) method is applied, resulting in residual errors whose upper bound can be defined using global TEC maps; More sophisticated TEC estimate techniques will enable more accurate IFB calibration in future work. As expected, the result shows that the temperature is the dominant effect on IFB variations in-orbit, and that calibration holds in-orbit during the mission.

I. INTRODUCTION

Bobcat-1, a 3-unit CubeSat developed and built within the Avionics Engineering Center at Ohio University, was launched on October 2nd, 2020 and deorbited on April 9th 2022, after a 17 month-long mission. The primary mission of Bobcat-1 was the estimation of Global Navigation Satellite System (GNSS) system-to-system time offsets (XYTOs) from low Earth orbit (LEO) using data collected by its onboard NovAtel OEM719. Bobcat-1 was deployed from the International Space Station (ISS) with an altitude of approximately $440\,\mathrm{km}$. The duration of one orbit was approximately 90 minutes, enabling the observation of multiple GNSS satellites multiple times per day. Aside from improved signal visibility, a receiver in LEO has additional advantages in

terms of measurement accuracy: it is not affected by tropospheric delay and multipath is negligible. Ionospheric delay must still be considered as the CubeSat orbited approximately within the most electron-dense part of the ionosphere's F2 region (Klobuchar, 1996). Additionally, the temperature of receiver in orbit was highly variable which introduces temperature-dependent biases within the receiver.

In Arnett et al. (2022), an initial analysis of XYTO was conducted with a focus on the Galileo-to-GPS time offset (GGTO). The results demonstrated XYTO estimates with stability of better than $3\,\mathrm{ns}$ over a period of several months. This analysis did not attempt to correct for temperature-induced variations in the measurements and the results exhibited oscillations that appear to indicate a correlation between receiver temperature and the estimates of XYTOs. In Ugazio et al. (2023), the analysis was expanded to include GLONASS and BeiDou where similar results were shown, with stability better than $5\,\mathrm{ns}$.

One challenge involved in accurately estimating XYTOs relates to the calibration of a specific receiver's own measurement biases. Dual-frequency ionospheric delay estimates are also affected by inter-frequency and inter-code biases present in both the GNSS satellites and the receiver. Accordingly, these biases must be calibrated or known in order to accurately determine ionospheric delay present in the LEO receiver's measurements. Each of these error sources also directly impact the estimation of XYTOs. Bobcat-1's receiver was tested using a temperature-controlled climate chamber on the ground with an identical NovAtel OEM719 before launch to facilitate the calibration of its inter-frequency biases (IFBs).

The objective of the work described in this paper is to calibrate the receiver-specific IFB. Given the wide range of temperature variations that Bobcat-1 experienced in orbit, the temperature effects on the receiver IFB need to be characterized as well. The calibration process applied here involves the use of data collected in a laboratory environment prior to launch to determine the temperature-dependent effect induced on the receiver IFB. Next, the results of this calibration are applied to data collected in-orbit for verification purposes. Then, in order to form an estimate of the absolute receiver IFB at a reference temperature, a zero-total electron content (TEC) calibration is applied in-orbit data. In this approach, an assumption that the ionospheric delay approaches zero during the time just before dawn is made (Rideout & Coster, 2006). In future work, more accurate ionospheric modeling techniques can be applied to enhance the estimate of the receiver IFB.

II. DOUBLE-FREQUENCY IONOSPHERIC DELAY ESTIMATE

As mentioned above, the ultimate goal of Bobcat-1 is to perform accurate estimation of XYTO. However, the effect of the ionosphere is still present in LEO and must be corrected for in order to form an accurate estimate. A typical dual-frequency ionospheric correction is computed by using pseudorange measurements from two frequencies (Hegarty et al., 2017, p. 638):

$$\tilde{I}^k_{f_1} = \frac{\rho_{f_1} - \rho_{f_2}}{1 - (f_1/f_2)^2} \tag{1}$$

Where:

- $\tilde{I}^k_{f_i}$ is the estimated ionospheric delay for satellite k on frequency f_i (m),
- ρ_{f_i} is the pseudorange measurement for satellite k on frequency f_i (m),
- f_i is the carrier frequency (Hz),

However, the ionosphere delay estimate calculated in Equation 1 includes not only the true ionospheric delay $I^k_{f_i}$, but impairments dominated by receiver and satellite biases; therefore, $\tilde{I}^k_{f_i}$ can be expressed, as modeled in (Grewal et al., 2020, p. 261), as:

$$\tilde{I}^k_{f_1} = I^k_{f_1} + \underbrace{c(\varepsilon^k_{f_1} - \varepsilon^k_{f_2})}_{\text{satellite DCB}} + \underbrace{\frac{c\big(\varepsilon_{f_{1,\mathrm{RX}}} - \varepsilon_{f_{2,\mathrm{RX}}}\big)}{1 - (f_1/f_2)^2}}_{\text{receiver-specific IFB}} \tag{2}$$

Where:

- $I^k_{f_i}$ is the true ionospheric delay for satellite k on frequency f_i (m),
- $\varepsilon^k_{f_i}$ is the satellite-specific frequency-dependent bias for satellite k on frequency f_i (ns),
- $\varepsilon_{f_{i,\mathrm{RX}}}$ is the receiver-specific inter-frequency-dependent bias on frequency f_i (ns),

The term differential code bias (DCB) has also been used in literature to describe the delay the signal experiences due to the specific hardware of the receiver at reception (Arikan et al., 2008). However, in this paper in order to clearly differentiate between the two, DCB will be used when describing the signal- and frequency-dependent delays imposed by the satellite, and IFB will be

used when discussing the frequency-dependent delays caused by the receiver hardware. The third component in Equation 2 is what is referred to as the receiver-specific IFB, whose calibration is the goal of this work.

III. SATELLITE DCB

Satellite differential code biases (DCBs), affecting the ionospheric estimate as in 2, are both signal- and frequency-dependent delays induced by the specific path the signals experience in the space vehicle (SV) hardware prior to transmission (Håkansson et al., 2016). Ideally, the generation of signals across all frequencies being broadcast by the satellite would happen simultaneously, however delays arise due to imperfections or limitations of the satellite instrumentation. The DCBs are known to be satellite-specific due to hardware variations, even among SVs of the same manufacturer and generation.

The satellite-specific DCBs are estimated and published as part of the International GNSS Service (IGS) Multi-GNSS Experiment (MGEX) by two analysis groups. The Institute of Geodesy and Geophysics (IGG) at the Chinese Academy of Sciences (CAS) and the German Aerospace Center DLR both publish independent estimates of the satellite and station biases in the Bias SINEX format (BSX) (Montenbruck et al., 2014), which can be downloaded via NASA's Archive of Space Geodesy Data (CDDIS) ((Noll, 2010). The DCB estimation method is detailed for each of the two analysis groups respectively by Wang et al. (2015) and Montenbruck et al. (2014).

IV. TEMPERATURE-DEPENDENT EFFECTS ON RECEIVER IFB

The receiver-specific IFB depends on factors such as the receiver analog hardware, correlator type and spacing, and tracking loop design (Hegarty et al., 2005). As shown in Equation 2, an accurate absolute measurement of the IFB requires accurate estimates of the DCBs and of the true ionospheric delay. The receiver-specific IFB is additionally temperature-dependent, which can be modeled as:

$$\text{IFB} = \overline{\text{IFB}} + f(T) \tag{3}$$

Where:

- IFB is the receiver-specific IFB,
- $\overline{\text{IFB}}$ is the receiver-specific IFB at reference temperature T_{REF},
- $f(T)$ is a function describing the temperature-induced variations of the receiver IFB,

1. Zero-Baseline Temperature Calibration Approach

Two nominally identical receivers, of the same make and model, are used in a zero-baseline configuration as represented in Figure 1, keeping one of the two at a reference temperature and the other one in a temperature chamber, subject to controlled temperature. Since only one temperature chamber is available at the Avionics Engineering Center, the receiver at reference temperature is at room temperature in the lab. Both receivers are equipped with onboard temperature sensors allowing for the characterization of the temperature-dependent variations of the receiver-specific IFB.

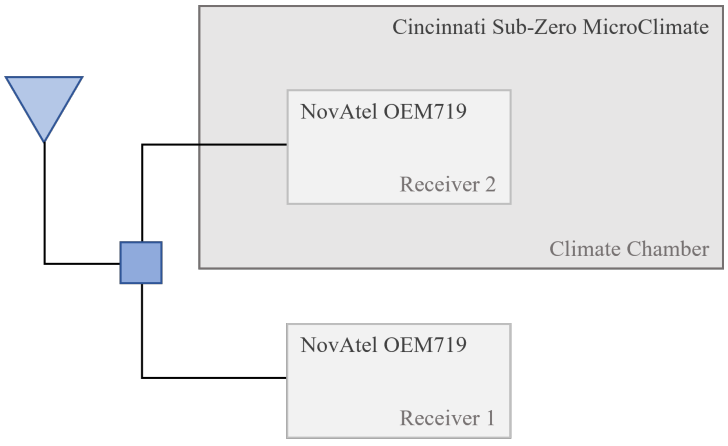

Figure 1: Zero-baseline test configuration

The assumption is that the two receivers are identical and at the same temperature the receiver-specific IFBs are the same. The

temperature-dependent variations of the receiver IFB are observed on the zero-baseline double-difference (Holaschutz et al., 2008):

$$\text{IRB} = (\rho^k_{f_1} - \rho^k_{f_2})_{\text{RX2}} - (\rho^k_{f_1} - \rho^k_{f_2})_{\text{RX1}} \tag{4}$$

Where the pseudorange measurement for satellite k on frequency f_i can be modeled, neglecting noise and multipath effects, as (Arikan et al., 2008):

$$\rho^k_{f_{i,\text{RXj}}} = R^k_{\text{RXj}} + c(\delta t_{\text{RXj}} - \delta t^k + \varepsilon^k_{f_i} + \varepsilon_{f_{i,\text{RXj}}}) + I^k_{f_{i,\text{RXj}}} + T^k_{\text{RXj}} + c\Delta_{f_{i,\text{RXj}}} \tag{5}$$

Where:

R^k	true range from satellite k,
$I^k_{f_i}$	ionospheric delay from satellite k on frequency i,
T^k	tropospheric delay from satellite k,
$\delta t_{\text{RX}j}$	clock offset of receiver j,
δt^k	satellite clock offset of satellite k,
$\varepsilon_{f_{i,\text{RX}j}}$	frequency-dependent bias of receiver j on frequency i,
$\varepsilon^k_{f_i}$	frequency-dependent bias of satellite k on frequency i,
$\Delta_{f_{i,\text{RX}j}}$	temperature-dependent delay of receiver j on frequency i

Therefore, the dual-frequency pseudorange difference for each receiver, involved in 4, can be written, respectively, as:

$$(\rho^k_{f_1} - \rho^k_{f_2})_{\text{RX1}} = I^k_{f_{1,\text{RX1}}} - I^k_{f_{2,\text{RX1}}} + c(\varepsilon^k_{f_1} - \varepsilon^k_{f_2}) + c(\varepsilon_{f_{1,\text{RX1}}} - \varepsilon_{f_{2,\text{RX1}}}) + c(\Delta_{f_{1,\text{RX1}}} - \Delta_{f_{2,\text{RX1}}}) \tag{6}$$

$$(\rho^k_{f_1} - \rho^k_{f_2})_{\text{RX2}} = \underbrace{I^k_{f_{1,\text{RX2}}} - I^k_{f_{2,\text{RX2}}}}_{\text{differential ionospheric delay}} + \underbrace{c(\varepsilon^k_{f_1} - \varepsilon^k_{f_2})}_{\text{satellite-specific DCB}} + \underbrace{c(\varepsilon_{f_{1,\text{RX2}}} - \varepsilon_{f_{2,\text{RX2}}}) + c(\Delta_{f_{1,\text{RX2}}} - \Delta_{f_{2,\text{RX2}}})}_{\text{receiver-specific IFB}} \tag{7}$$

It shall be noted that in Equations 6 and 7 the ionospheric terms, as well as the the DCB, are the same. Therefore they cancel out in the double difference in Equation 4, as expected, leading to a geometry free linear combination (Arikan et al., 2008). Indeed, substituting Equations 6 and 7 in Equation 4 the remaining terms are the difference between the IFB of the two receivers, and can be expressed in meters as:

$$\text{IRB}_{\text{RX2}-\text{RX1}} = c(\varepsilon_{f_1} - \varepsilon_{f_2})_{\text{RX2}} - c(\varepsilon_{f_1} - \varepsilon_{f_2})_{\text{RX1}} + c(\Delta_{f_1} - \Delta_{f_2})_{\text{RX2}} - c(\Delta_{f_1} - \Delta_{f_2})_{\text{RX1}} \tag{8}$$

where $c(\varepsilon_{f_1} - \varepsilon_{f_2})_{\text{RXi}}$ is the receiver-specific IFB of the i-th receiver at a reference temperature, and $c(\Delta_{f_1} - \Delta_{f_2})_{\text{RX}i}$ is the temperature-dependent bias of the i-th receiver.

In order to calibrate the temperature-induced changes in the IFB using this method, differences in the IFB of each receiver at a reference temperature need to be measured and taken into account. Therefore the temperature calibration procedure is made of two steps:

1. Inter-receiver bias (IRB) calibration, with both receivers at the same reference temperature, described in Section IV.2
2. Temperature-variations of the receiver-specific IFB characterization, with one receiver at a reference temperature and the other receiver subjected to controlled temperature variations, described in Section IV.3

2. Inter-Receiver Calibration

The IRB at a reference temperature measured in a zero-baseline configuration, while the two receivers at the same temperature $T_{\text{RX1}} = T_{\text{RX2}} = T_{\text{REF}}$ can be expressed as:

$$\overline{\text{IRB}}_{\text{RX2}-\text{RX1}} = c(\varepsilon_{f_1} - \varepsilon_{f_2})_{\text{RX2}} - c(\varepsilon_{f_1} - \varepsilon_{f_2})_{\text{RX1}} \tag{9}$$

Ideally, the IRB between the two receivers when they are at the same temperature is expected to be zero, due to the assumption that the receivers are identical and thus have identical IFBs. However, due to receiver hardware and temperature sensor inaccuracies, differences are observed.

3. Temperature Calibration

The temperature-induced effect on the receiver-specific IFB can be observed by keeping Receiver 1 at the reference temperature T_{REF} and subjecting Receiver 2 to temperature variations, T,

$$\text{IRB}_{\text{RX2}-\text{RX1}} = \overline{\text{IRB}}_{\text{RX2}-\text{RX1}} + c(\Delta_{f_2} - \Delta_{f_1})_{\text{RX2}}\Big|_{T} - c(\Delta_{f_2} - \Delta_{f_1})_{\text{RX1}}\Big|_{T_{\text{REF}}} \tag{10}$$

where $\overline{\text{IRB}}$ is the IRB estimated in IV.2.

V. RECEIVER-SPECIFIC IFB ESTIMATION

In order to calibrate the receiver-specific IFB, the true ionospheric delay $I^k_{f_i}$ in Equation 1 needs to be estimated. Different methods can be applied to estimate this delay (Coster et al., 2013). Here a basic method is applied as a starting point: the zero-TEC method. In this method, the ionospheric delay is assumed to be zero in the hours just before dawn (approximately 5:00-6:00 a.m. local Solar time (LST)). The zero-TEC method has been shown to be robust in non-equatorial areas, and is expected to be more effective at the Bobcat-1 altitude, where less of the ionosphere affects the measurements. It is expected to result in a residual bias, whose upper bound can be determined by comparison with the global TEC maps.

VI. LABORATORY RESULTS

The prior procedure is generic and can be applied to dual-frequency measurements from any GNSS constellation, although GLONASS will require special care as each SV transmits on a unique frequency. In order to validate our calibration technique, we consider only Galileo E1C (f_{E1C} =1575.42 MHz) and E5b (f_{E5bQ} =1207.14 MHz) and GPS L2P(Y) (semi-codeless) ($f_{\text{L2P(Y)}}$ =1227.6 MHz) and L5 (f_{L5} =1176.45 MHz) with the plan to apply this procedure to other constellations and signals in future work.

1. Satellite DCB

First of all, the DCB corrections need to be applied. The DCBs provided in the single day files published by DLR are used to mitigate the signal- and frequency-dependent satellite-specific DCBs from the geometry free linear combinations.

Figure 2 shows how removing the satellite DCBs impacts the difference in pseudorange measurements. After taking the difference of pseudorange measurements on two frequencies from the same SV, only errors that are frequency-dependent remain, such as the ionospheric delay, the satellite DCBs, and receiver-specific IFB (Equations 6 & 7). Once the satellite-specific DCBs have been removed, only the sum of the differential ionospheric path delay ($I^k_{f_1} - I^k_{f_2}$) and the receiver-specific IFB remain.

2. Calibration of Temperature Effects

By configuring the two receivers as shown in Figure 1 and subjecting one of the receivers to temperature variations using a climate chamber, while the other is kept at a reference temperature, variations of the receiver-specific IFB due to temperature were observed. Multiple data collections lasting up to three days each using different temperature profiles have been conducted in the lab, obtaining repeatable results. Some results are shown in this section. The top plot in Figure 3 shows one of temperature profiles measured by the receiver during testing in the temperature chamber, intentionally emulating the expected temperature changes expected in orbit. The bottom plot in Figure 3 shows the actual measured temperature during a data collection in orbit. It can be seen that the temperature profile selected for the pre-flight calibration more than covered the temperature-variations the receiver experienced on orbit.

Figure 4 shows the IRB, or the difference of Receiver 2's IFB and Receiver 1's IFB, in which temperature-dependent oscillations in the IRB can be seen, repeating periodically with the temperature periodic variations.

The IRB is plotted as a function of the temperature difference, $T - T_{\text{REF}}$, where $T_{\text{REF}} = 40.12°\text{C}$. Figure 5 shows a linear relationship between the temperature difference of the receiver with respect to T_{REF} and the IRB. To characterize the relationship between the IRB and the receiver's temperature, for every 2°C of temperature difference the average IRB was calculated and a line was fit to the average values. For Galileo E1C-E5b, the resulting line has a slope of $-0.0148\,\text{ns}/°\text{C}$ and a goodness of fit (R^2) value of 0.99462 (Figure 5). For GPS L2P(Y)(semi-codeless)-L5, the line has a slope of $\text{ns}/°\text{C}$ and an R^2 value of 0.9900. The linear approximation of the relationships was then applied to remove any temperature-induced effects in the IRB. Figure 4 shows both the uncalibrated IRB and the temperature-calibrated IRB for Galileo E1C-E5b using the same data collection that was used to characterize the temperature effects. To validate the result, a different data collection was considered and the temperature calibration was applied. Similar results were obtained for GPS L2P(Y)(semi-codeless)-L5.

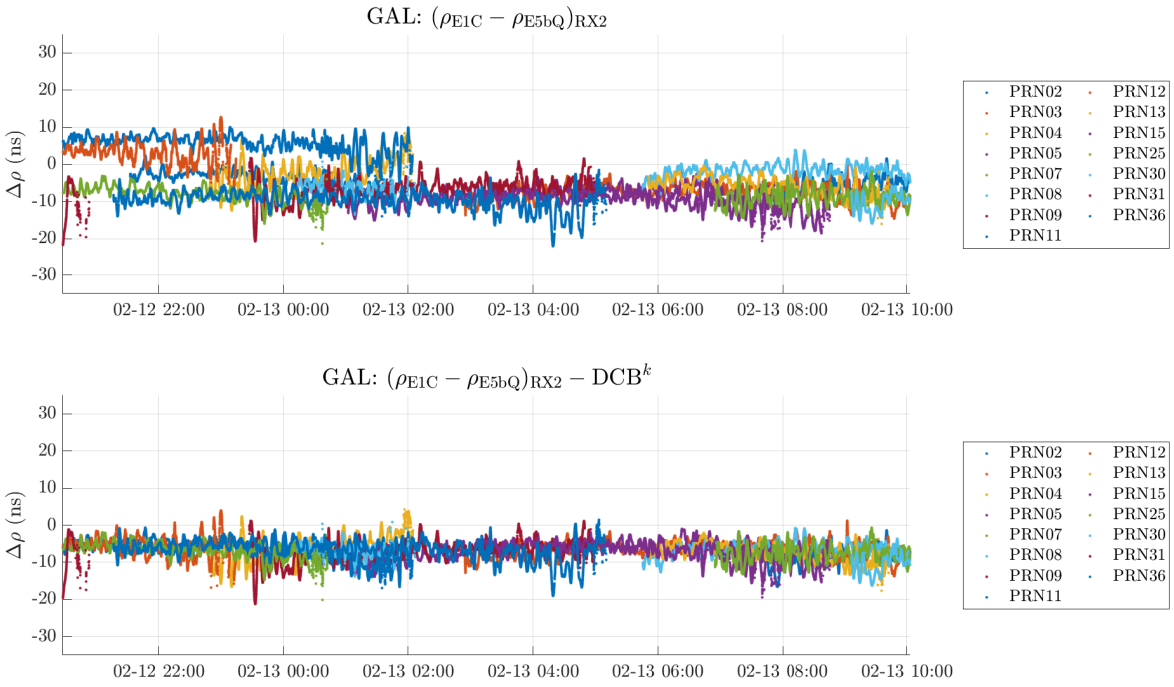

Figure 2: Difference of pseudoranges on Galileo E1C and E5b: uncorrected (top) and with satellite DCBs removed (bottom)

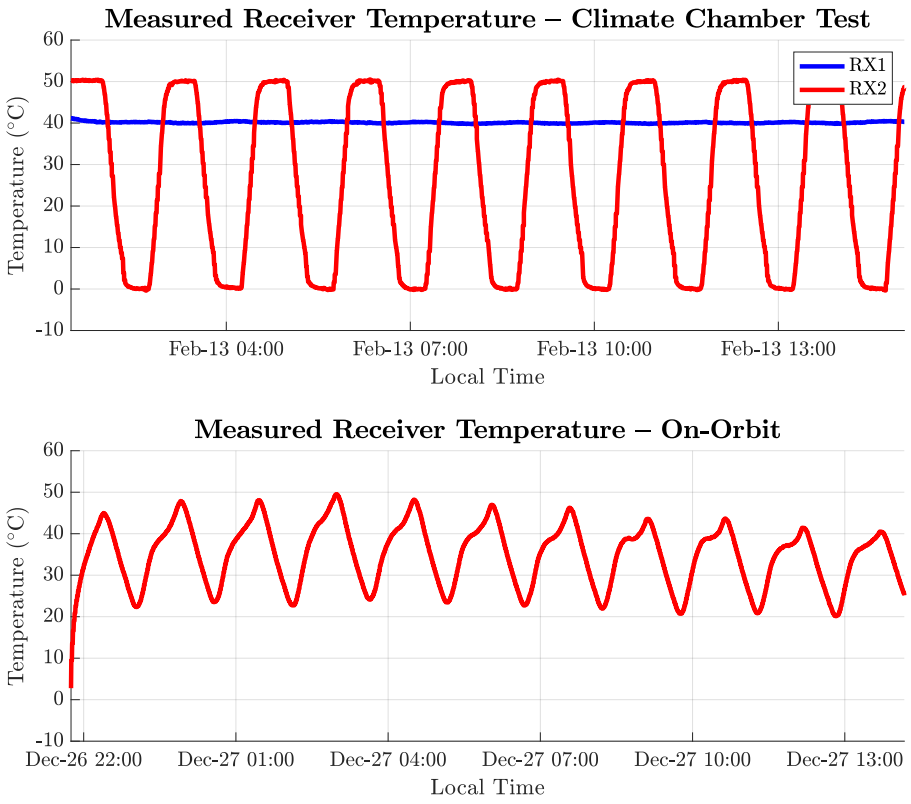

Figure 3: The measured receiver temperatures during a climate-chamber test prior to launch (top) and the measured receiver temperature during a data collection on-orbit (bottom)

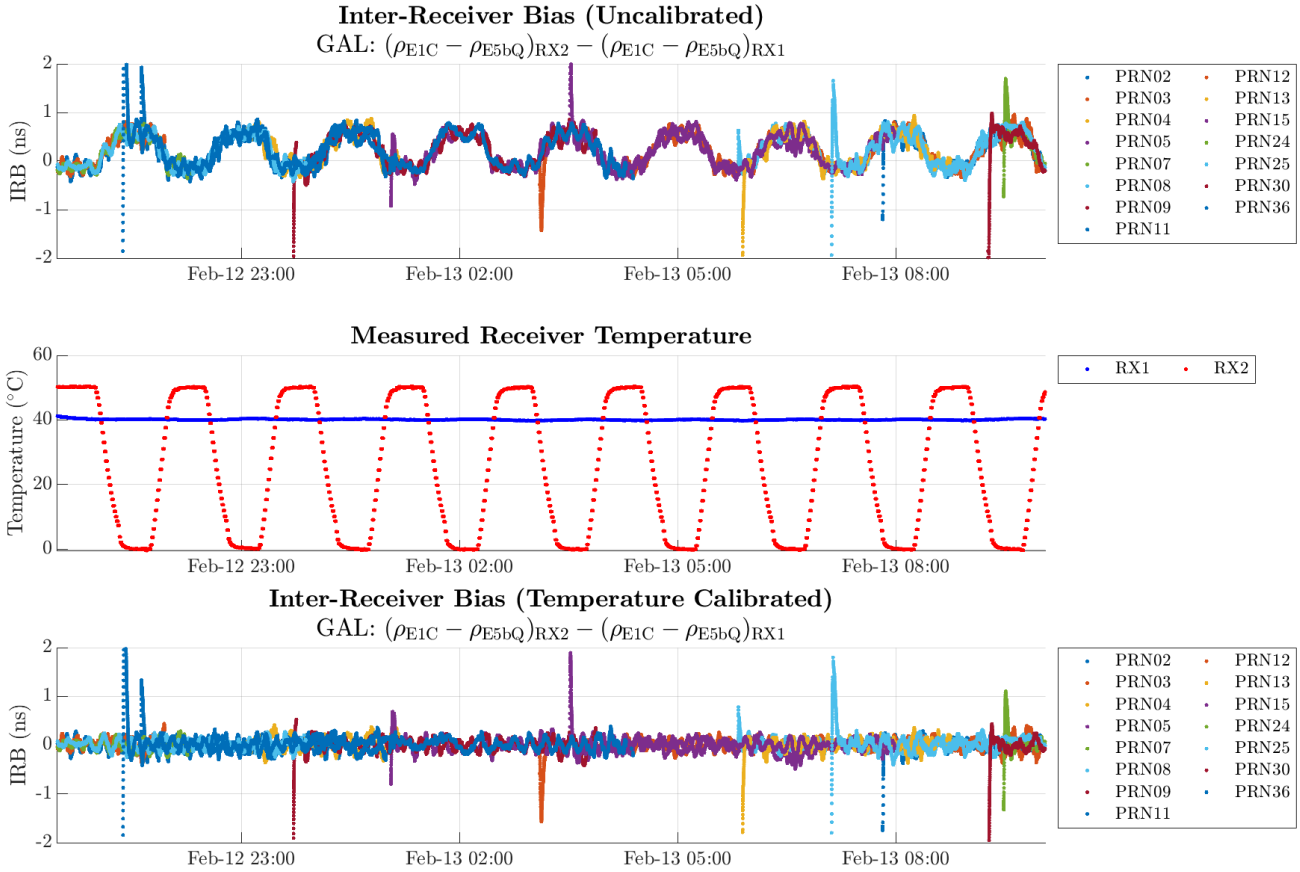

Figure 4: Uncalibrated inter-receiver bias between RX1 and RX2 (top), measured receiver temperature (middle), and calibrated inter-receiver bias between RX1 and RX2 (bottom)

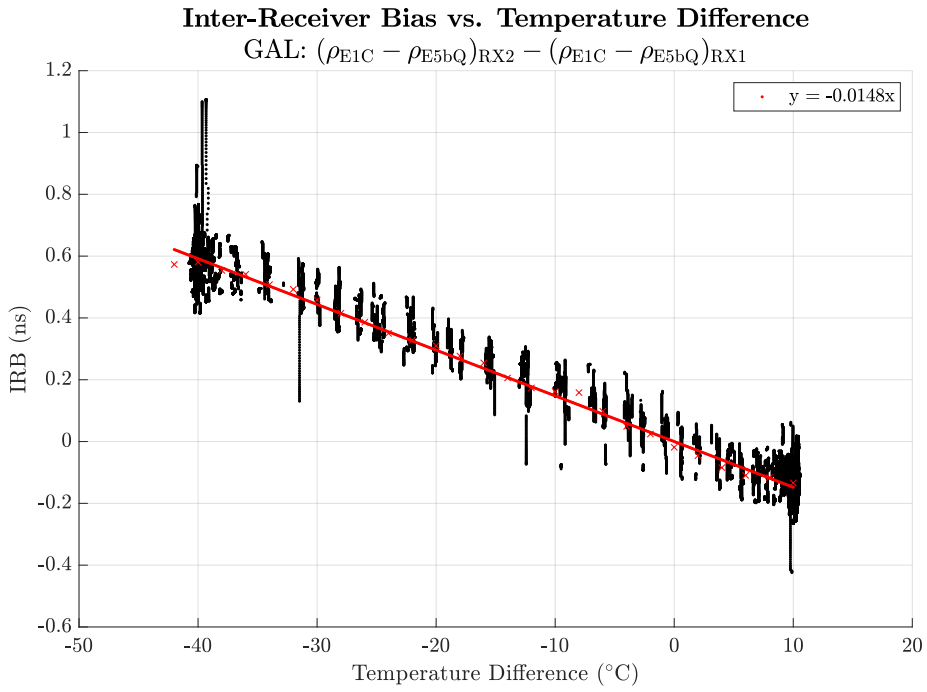

Figure 5: Inter-receiver bias between RX1 and RX2 (top) and measured receiver temperature (bottom)

VII. ON-ORBIT VALIDATION AND ZERO-TEC CALIBRATION

The key-part of this work is the on-orbit validation of the temperature calibration done in the laboratory prior to launch, to verify that it holds in space. Several on-orbit data collections are considered here, ranging from September of 2021 to February of 2022 (details provided in Table 1). The dual-frequency pseudorange differences are calculated, satellite DCBs are removed and temperature calibration is applied. The remaining effects are the ionospheric effect and the IFB at a reference temperature. In order to separate the ionospheric delay and the receiver-specific IFB the zero-TEC calibration technique is applied. Since the zero-TEC method is based on the assumption that the minimum TEC, usually occurring just before dawn, can be approximated to be zero, the focus is on the measurements taken during the 5:00-6:00 a.m. time frame.

To plot the data as a function of the local time, the data is then sorted by the LST corresponding to the longitude of Bobcat-1 when the measurement was made. In sorting the data by LST instead of chronologically, an observation of the receiver-specific IFB can be made during the 5-6 a.m. time frame when it is assumed that there is zero ionospheric delay. Figure 6 shows the double-frequency pseudorange difference for Galileo E1C and E5b, plotted with respect to the local solar time, for data collection 174, whose duration was about 24 hours. The upper plot in Figure 6 is the uncalibrated difference, while in the lower plot the IFB temperature variations as well the DCBs are calibrated. Different colors correspond to different satellites, and it can be seen how the DCB calibration reduces the variations between satellites, while here the effect of the temperature calibration is not dominant at first sight, since the effect of the ionosphere is dominant.

Figure 7 shows the same plots as in Figure 6, zoomed between 4:00 a.m. and 7:00 a.m. LST. Assuming that during this time interval the ionospheric effect was not present leads to an estimate of the receiver-specific IFB at the reference temperature, approximately $6\,\mathrm{ns}$. However, observing how spread the values are still, it is obvious that some ionospheric effect was present. Therefore, in order to have a more accurate estimate of the receiver IFB a more accurate estimate of the ionospheric effect is necessary, using either the in orbit or the laboratory data. A mapping function to estimate the vertical TEC could be applied, or a gradient algorithm.

Figure 8 and 9 show the same results, for Collection 181, whose length was also around 24 hours. After more than a month from the previous data collection (see Table 1), the IFB estimated applying a zero-TEC method lead to a similar result, of about $6\,\mathrm{ns}$, suggesting that the receiver-specific IFB may be the dominant effect over residual ionospheric effects.

Figures 10, 11 and 12, 13 show similar results for collections 174 and 181 respectively, considering GPS L2P(Y) (semi-codeless) and L5. The result is similar, leading to an estimated residual IFB of about $4\,\mathrm{ns}$ in both the collections, despite them being more than a month apart.

While the plots are shown for only two data collections, Table 2 and Table 3 summarize the zero-TEC estimated receiver-specific IFB (at reference temperature) in the five data collections described in Table in 1. Further analysis and more accurate ionospheric estimates are needed, but this result already shows sub-nanosecond stability.

Table 1: On-Orbit Data Collection Details

Collection ID	Start Date	Start Time	End Date	End Time	Duration
170	September 28th, 2021	20:11:02 UTC	September 29th, 2021	16:44:22 UTC	20:33:20
174	November 10th, 2021	03:30:42 UTC	November 11th, 2021	01:08:22 UTC	21:37:40
176	November 29th, 2021	23:09:22 UTC	November 30th, 2021	17:36:42 UTC	18:27:20
181	December 26th, 2021	21:50:22 UTC	December 27th, 2021	14:10:22 UTC	16:20:20
215	February 27th, 2022	12:01:22 UTC	February 28th, 2022	11:59:22 UTC	23:58:00

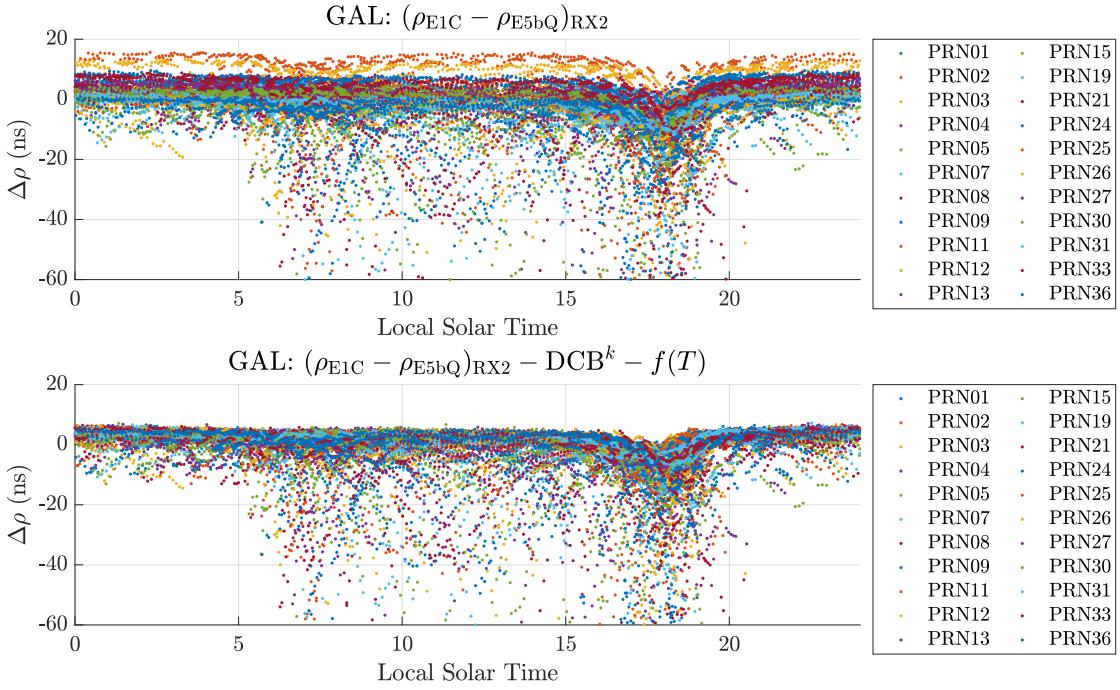

Figure 6: Collection ID 174: Difference of pseudoranges on GAL E1C and E5b uncorrected (top) and with DCBs and temperature-variations in receiver-specific IFB removed

VIII. CONCLUSIONS AND FUTURE WORK

The objective of this work is the calibration of the receiver-specific IFB in order to accurately estimate the ionospheric delay using double-frequency difference measurements, with the ultimate goal of improving the accuracy of the XYTO estimates made using data collections from Bobcat-1. The calibration procedure was described, and the results shown for Galileo E1C-E5b and GPS L2P(Y) (semi-codeless)-L5. The receiver-specific IFB temperature variations were calibrated and their validity was proven in orbit; the application of the calibration, together with the DCB, led to the opportunity of an on-orbit zero-TEC calibration to estimate the receiver-specific IFB at a reference temperature. Despite residual ionospheric effects are present, showing that the zero-TEC assumption is not accurate, comparison between five data collections over a six-month time-span shows stability on the IFB estimate within $1\,\mathrm{ns}$. Further analysis to better estimate or model the true ionospheric delay will enable higher accuracy of the receiver IFB estimate. More advanced ionospheric estimation methods such as the improved zero-TEC method (Zhong et al., 2016), using global TEC maps, or a gradient algorithm (Bourne & Morton, 2013). In future work, this calibration technique will be expanded to other GNSSs and signal/frequency combinations. Calibrated ionospheric corrections will be formed and XYTOs will be estimated using corrected pseudorange measurements.

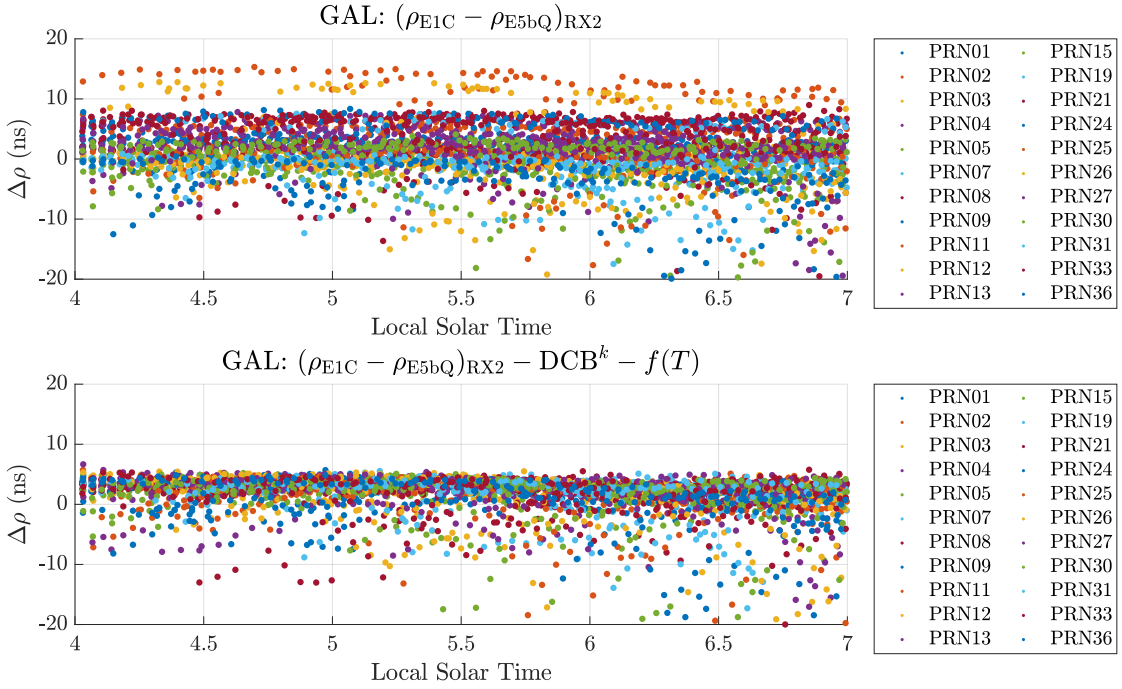

Figure 7: Collection ID 174: Difference of pseudoranges on GAL E1C and E5b uncorrected (top) and with DCBs and temperature-variations in receiver-specific IFB removed, focused on the 4:00-7:00 a.m. time frame

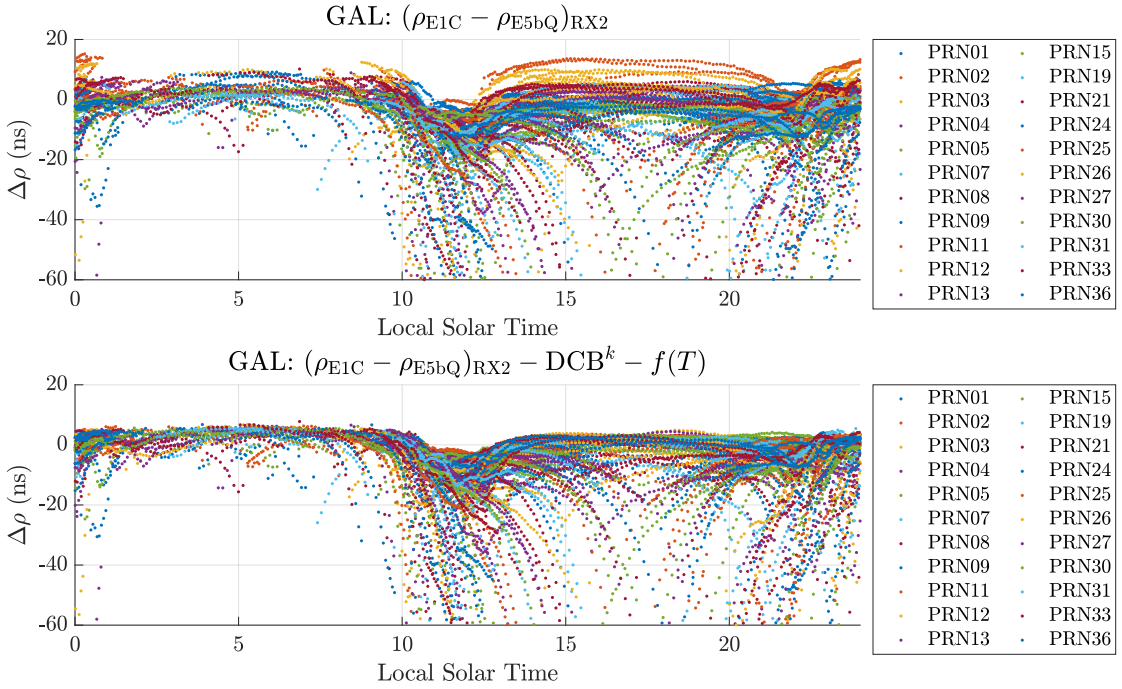

Figure 8: Collection ID 181: Difference of pseudoranges on GAL E1C and E5b uncorrected (top) and with DCBs and temperature-variations in receiver-specific IFB removed

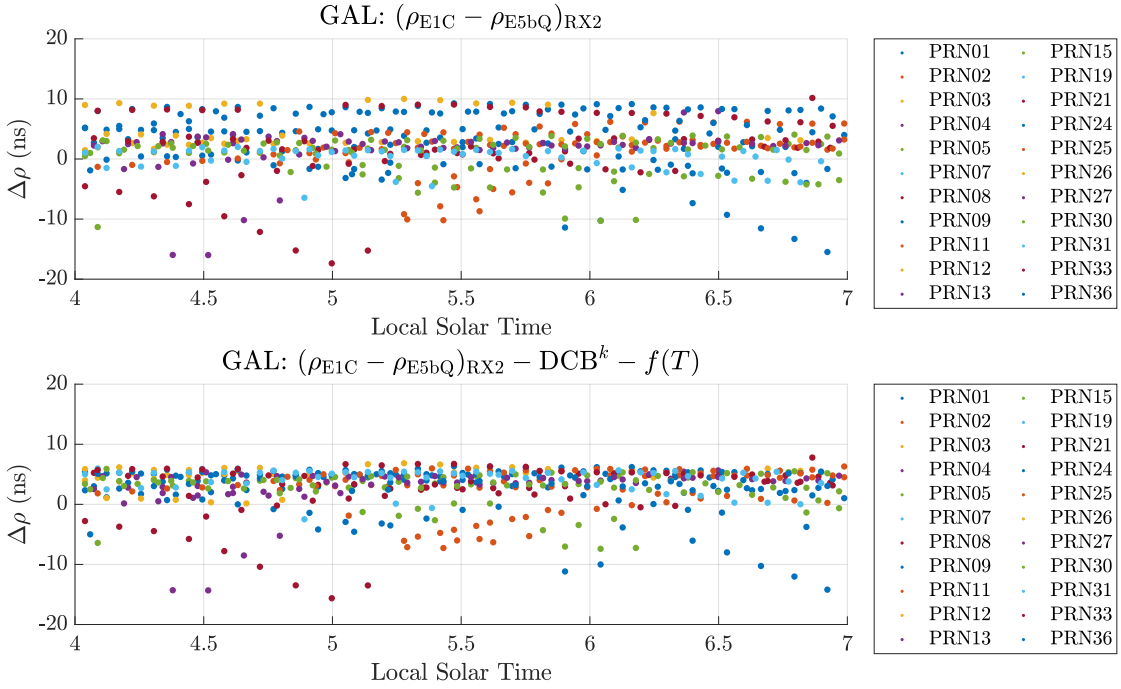

Figure 9: Collection ID 181: Difference of pseudoranges on GAL E1C and E5b uncorrected (top) and with DCBs and temperature-variations in receiver-specific IFB removed, focused on the 4:00-7:00 a.m. time frame

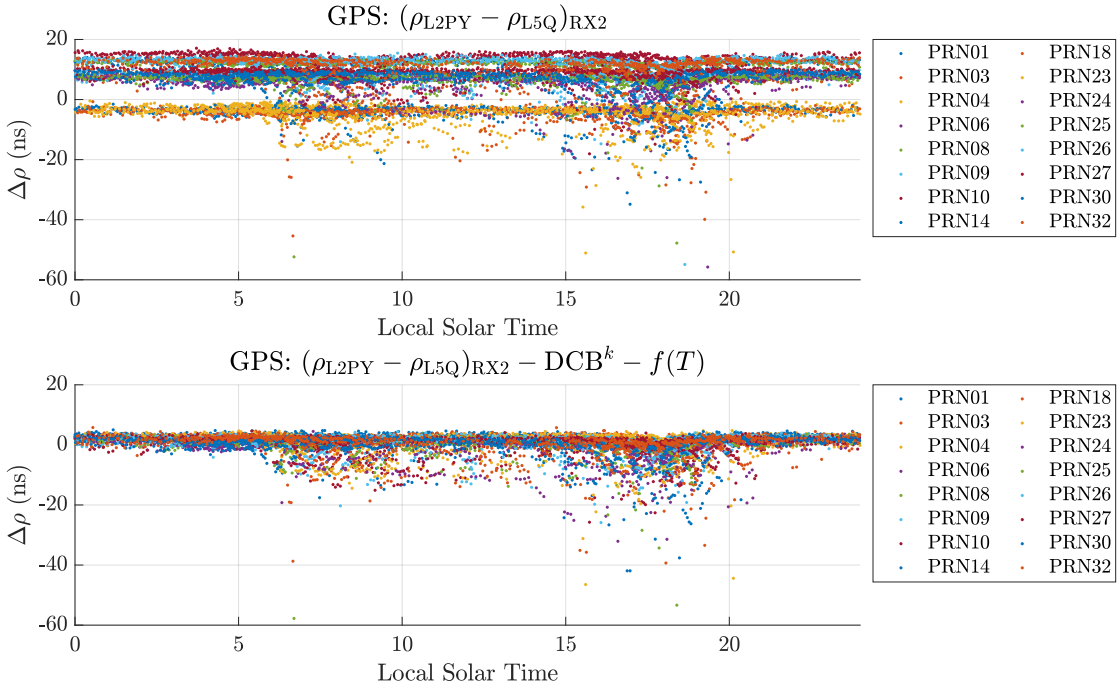

Figure 10: Collection ID 174: Difference of pseudoranges on GPS L2P(Y) semi-codeless and L5 uncorrected (top) and with DCBs and temperature-variations in receiver IFB removed

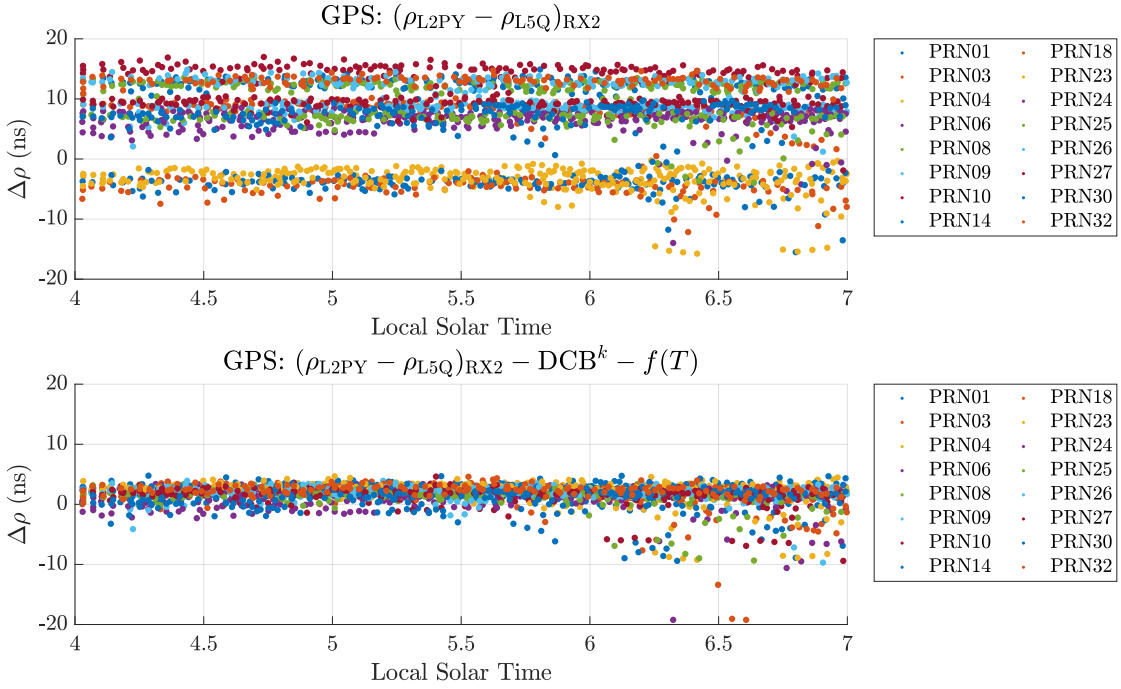

Figure 11: Collection ID 174: Difference of pseudoranges on GPS L2P(Y) semi-codeless and L5 uncorrected (top) and with DCBs and temperature-variations in receiver IFB removed, focused on the 4:00-7:00 a.m. time frame

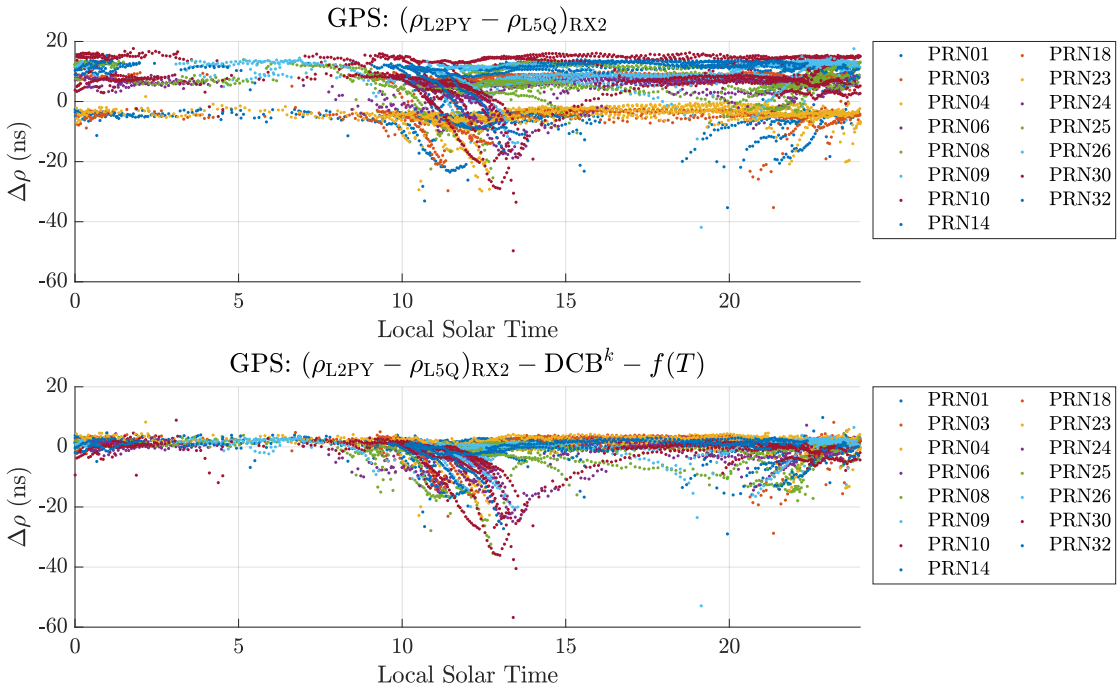

Figure 12: Collection ID 181: Difference of pseudoranges on GPS L2P(Y) semi-codeless and L5 uncorrected (top) and with DCBs and temperature-variations in receiver IFB removed

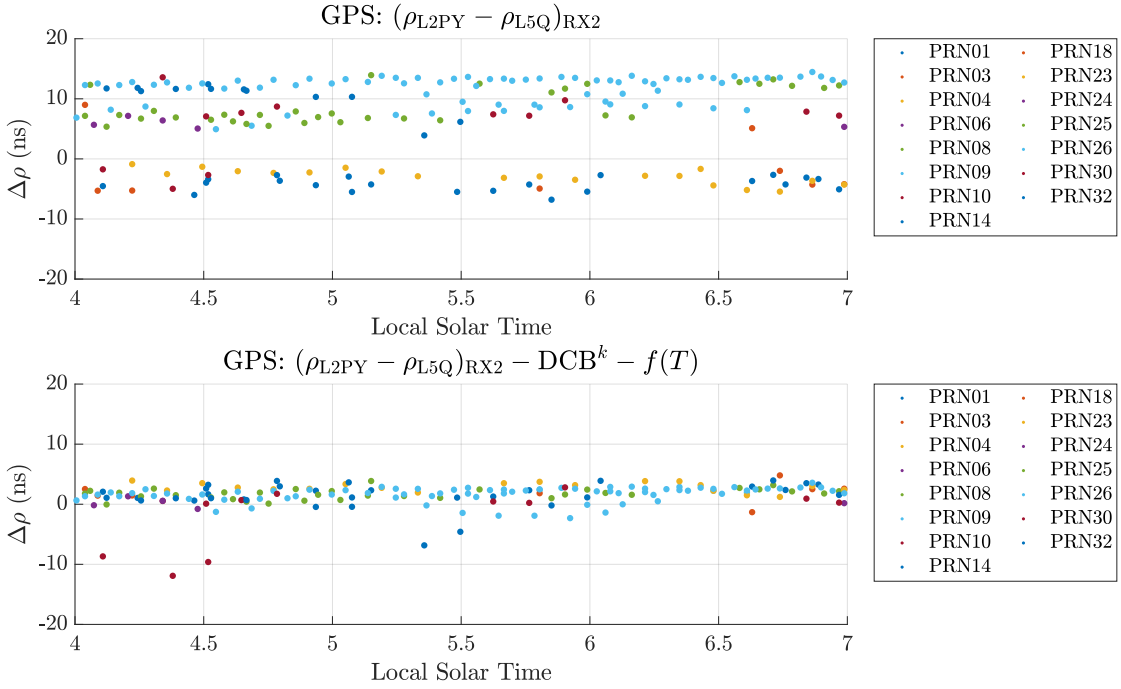

Figure 13: Collection ID 181: Difference of pseudoranges on GPS L2P(Y) semi-codeless and L5 uncorrected (top) and with DCBs and temperature-variations in receiver IFB removed, focused on the 4:00-7:00 a.m. time frame

Table 2: Receiver-Specific Inter-Frequency Bias Estimates for GAL $\rho_{\text{E1C}} - \rho_{\text{E5b}}$

Collection ID	Estimated IFB
170	6.175 ns
174	5.022 ns
176	5.781 ns
181	5.936 ns
215	5.499 ns
Average	5.683 ns
Std	0.443 ns

Table 3: Receiver-Specific Inter-Frequency Bias Estimates for GPS $\rho_{\text{L2P(Y)}} - \rho_{\text{L5}}$

Collection ID	Estimated IFB
170	4.508 ns
174	4.217 ns
176	3.747 ns
181	3.498 ns
215	3.985 ns
Average	3.991 ns
Std	0.394 ns

ACKNOWLEDGMENTS

The authors would like to acknowledge NASA's Satellite Communication and Navigation office (SCaN), NASA Glenn Research Center, NASA's CubeSat Launch Initiative (CSLI) and Ohio University for funding the Bobcat-1 CubeSat mission. Additionally, Kevin Croissant and Gregory Jenkins, previous student members of the Bobcat-1 Team, Austin McKibben, for supporting in-orbit operations for the CubeSat mission, and Dr. Frank van Graas, Ohio University Professor Emeritus and former faculty member of the Bobcat-1 team.

REFERENCES

Arikan, F., Nayir, H., Sezen, U., & Arikan, O. (2008). Estimation of single station interfrequency receiver bias using GPS-TEC. *Radio Science*, *43*(4). https://doi.org/10.1029/2007rs003785

Arnett, Z., McKnight, R., Ugazio, S., & van Graas, F. (2022). Receiver inter-constellation time offset at low Earth orbit: An experiment with Bobcat-1, the Ohio University CubeSat. *Proceedings of the 2022 International Technical Meeting (ION ITM 2022)*, 844–855. https://doi.org/10.33012/2022.18176

Bourne, H., & Morton, Y. (2013). GPS receiver ionosphere error correction based on spatial gradients and IGS satellite DCBs. *Proceedings of the ION 2013 Pacific PNT Meeting*, 685–693.

Coster, A., Williams, J., Weatherwax, A., Rideout, W., & Herne, D. (2013). Accuracy of GPS total electron content: GPS receiver bias temperature dependence. *Radio Science*, *48*(2), 190–196. https://doi.org/10.1002/rds.20011

Grewal, M. S., Andrews, A. P., & Bartone, C. G. (2020). *Global navigation satellite systems, inertial navigation, and integration* (4th ed.). Wiley.

Håkansson, M., Jensen, A. B. O., Horemuz, M., & Hedling, G. (2016). Review of code and phase biases in multi-GNSS positioning. *GPS Solutions*, *21*(3), 849–860. https://doi.org/10.1007/s10291-016-0572-7

Hegarty, C. J., Kaplan, E. D., Uijt de Haag, M., & Cosention, R. (2017). GNSS errors. In E. D. Kaplan & C. J. Hegarty (Eds.), *Understanding GPS/GNSS: Principles and applications* (3rd ed., pp. 619–660). Artech House.

Hegarty, C. J., Powers, E. D., & Fonville, B. (2005). Accounting for timing biases between GPS, modernized GPS, and GALILEO signals. *Proceedings of the 18th International Technical Meeting of the Satellite Division of The Institute of Navigation (ION GNSS 2005)*, 2401–2407.

Holaschutz, D., Bishop, R. H., Harris, R. B., & Tolman, B. (2008). Inter-frequency bias estimation for the GPS monitor station network. *Proceedings of the 21st International Technical Meeting of the Satellite Division of The Institute of Navigation (ION GNSS 2008)*, 2405–2415.

Klobuchar, J. A. (1996). *Ionospheric effects on GPS* (B. W. Parkinson & J. J. Spilker Jr., Eds.; Vol. 1). American Institute of Aeronautics; Astronautics, Inc.

Montenbruck, O., Hauschild, A., & Steigenberger, P. (2014). Differential code bias estimation using multi-GNSS observations and global ionosphere maps. *NAVIGATION: Journal of the Institute of Navigation*, *61*(3), 191–201. https://doi.org/10.1002/navi.64

Noll, C. E. (2010). The crustal dynamics data information system: A resource to support scientific analysis using space geodesy. *Advances in Space Research*, *45*(12), 1421–1440. https://doi.org/10.1016/j.asr.2010.01.018

Rideout, W., & Coster, A. (2006). Automated GPS processing for global total electron content data. *GPS Solutions*, *10*(3), 219–228. https://doi.org/10.1007/s10291-006-0029-5

Ugazio, S., Arnett, Z., McKnight, R., & Peters, B. C. (2023). Receiver-specific GNSS inter-system bias in low earth orbit. *Proceedings of the 2023 International Technical Meeting of The Institute of Navigation*, 831–843. https://doi.org/10.33012/2023.18678

Wang, N., Yuan, Y., Li, Z., Montenbruck, O., & Tan, B. (2015). Determination of differential code biases with multi-GNSS observations. *Journal of Geodesy*, *90*(3), 209–228. https://doi.org/10.1007/s00190-015-0867-4

Zhong, J., Lei, J., Yue, X., & Dou, X. (2016). Determination of differential code bias of GNSS receiver onboard low earth orbit satellite. *IEEE Transactions on Geoscience and Remote Sensing*, *54*(8), 4896–4905. https://doi.org/10.1109/tgrs.2016.2552542